A Generalized Active Learning Approach for Unsupervised Anomaly Detection

Tiago Pimentel
Kunumi
Belo Horizonte, Brazil
tiago.pimentel@kunumi.com

Marianne Monteiro
Kunumi
Belo Horizonte, Brazil
marianne@kunumi.com

Juliano Viana
Kunumi
Belo Horizonte, Brazil
juliano@kunumi.com

Adriano Veloso
CS Dept@UFMG
Belo Horizonte, Brazil
adrianov@dcc.ufmg.br

Nivio Ziviani
CS Dept@UFMG & Kunumi
Belo Horizonte, Brazil
nivio@dcc.ufmg.br

Abstract

This work formalizes the new framework for anomaly detection, called *active anomaly detection*. This framework has, in practice, the same cost of unsupervised anomaly detection but with the possibility of much better results. We show that unsupervised anomaly detection is an undecidable problem and that a prior needs to be assumed for the anomalies probability distribution in order to have performance guarantees. Finally, we also present a new layer that can be attached to any deep learning model designed for unsupervised anomaly detection to transform it into an active anomaly detection method, presenting results on both synthetic and real anomaly detection datasets.

1 Introduction

Anomaly detection (a.k.a. outlier detection) [Aggarwal, 2015, Chandola et al., 2009, Hodge and Austin, 2004] aims to discover rare instances that do not conform to the patterns of majority. It has been amply studied in recent works [Li et al., 2017, Liu et al., 2017, Maurus and Plant, 2017, Perozzi et al., 2014, Siffer et al., 2017, Zheng et al., 2017, Zhou and Paffenroth, 2017, Zong et al., 2018], with solutions inspired by extreme value theory [Siffer et al., 2017], robust statistics [Zhou and Paffenroth, 2017] and graph theory [Perozzi et al., 2014].

Unsupervised anomaly detection is a sub-area of outlier detection which aims to discover these rare instances in an already 'contaminated' dataset. It is a specially hard task, where there is usually no information on what these rare instances are and most works use heuristics/approximations to discover these anomalies, providing an anomaly score $s(x)$ for each instance in this dataset.

In this work, we first show that unsupervised anomaly detection is an undecidable problem, requiring priors to be assumed on the anomaly distribution; we then argue in favor of a new approach to anomaly detection, called *active anomaly detection* (Section 2). We propose a new learning layer, called here Universal Anomaly Inference (UAI), that can be applied on top of any unsupervised anomaly detection system based on deep learning to transform it in an *active anomaly detection system* (Section 3). We also present experiments showing the performance of our active systems vs unsupervised/semi-supervised ones under similar budgets in both synthetic and real datasets (Section 4). Finally, we visualize our models learned latent representations, comparing them to unsupervised models' ones and analyze our model's performance for different numbers of labels (Appendix C).

Preprint. Work in progress.

2 Problem Definition

Grubbs [1969] defines an outlying observation, or outlier, as one that appears to deviate markedly from other members of the sample in which it occurs. Hawkins [1980] states that an outlier is an observation that deviates so much from other observations as to arouse suspicion that it was generated by a different mechanism. While Chandola et al. [2009] says that normal data instances occur in high probability regions of a stochastic model, while anomalies occur in the low probability regions of the stochastic model.

Following these definitions, specially the one from [Hawkins, 1980], we assume there is a probability density function from which our 'normal' data instances are generated:

$$X_{normal} \sim p_{normal}\left(x\right) = p\left(x|y=0\right) \tag{1}$$

where x is an instance's available information[1] and y is a label saying if the point is anomalous or not. There is also a different probability density function from which anomalous data instances are sampled:

$$X_{anom} \sim p_{anom}\left(x\right) = p\left(x|y=1\right) \tag{2}$$

In this problem, a dataset would be composed of both normal and anomalous instance, being sampled from a probability distribution that follows:

$$\begin{array}{rcccl} (X,Y)_{full} & \sim & p_{full}\left(x,y\right) & = & p\left(y\right)p\left(x|y\right) \\ X_{full} & \sim & p_{full}\left(x\right) & = & p\left(y=0\right)p_{normal}\left(x\right) + p\left(y=1\right)p_{anom}\left(x\right) \\ & & & = & (1-\lambda)p_{normal}\left(x\right) + \lambda p_{anom}\left(x\right) \end{array} \tag{3}$$

where λ is an usually small constant representing the probability of a random data point being anomalous ($\lambda = p(y=1)$), this constant can be either known a priori or not.

Chandola et al. [2009] divides anomaly detection learning systems in three different types:

- Supervised: You are given curated training/test sets where labels of normal/anomalous instances are known. This case is similar to an unbalanced supervised classification setting:
$$\mathcal{D}_{train/test} = (X,Y)_{train/test} \sim p_{full}(x,y)$$
- Semi-Supervised: You are given a curated training set which only contains normal instances and need to identify anomalous instances in a test set. This problem can also be called novelty detection:
$$\mathcal{D}_{train} = X_{train} \sim p_{normal}(x)$$
$$\mathcal{D}_{test} = X_{test} \sim p_{full}(x)$$
- Unsupervised: You are given a dataset which contains both normal and anomalous instances and must find the anomalous instances in it. There is no concept of a test set since anomalous instances must be sorted in the dataset itself:
$$\mathcal{D} = X \sim p_{full}(x)$$

2.1 Unsupervised Anomaly Detection

In this work we will focus on *unsupervised anomaly detection*. In this problem, then, there is a dataset $\mathcal{D} = \{X\}$ composed of both normal and anomalous instances. Having this set of datapoints X we want to find a subset $X_{anom} \subset X$ which is composed of the anomalous instances.

The probability distribution p_{full} is a mixture of distributions and Dasgupta et al. [2005] states that, for a mixture of distributions that overlap very closely, it may be impossible to learn the individual distributions beyond a certain accuracy threshold. In the sequence we show that it is impossible to recover p_{anom} from p_{full} for any small λ without a prior on the anomalies probability distribution.

[1] x, in our notation, is the information known about a data instance. This can be further composed of what would actually be x and y in a supervised setting, such as an image and its corresponding class label. We will reference this as x_x and x_y here.

Lemma 1. ***Mixture probability lemma.*** *Consider two independent arbitrary probability distributions p_1 and p_2. Given only a third distribution $p_+ = \overline{p}$ composed of the weighted average of the two:*

$$p_+ = (1 - \lambda) \cdot p_1 + \lambda \cdot p_2, \quad 0 \leq \lambda \leq 1$$

and considering P_i as the residual probability distribution hyperplanes:

$$\begin{aligned} P_1 &= \left\{ p_r = \tfrac{\overline{p} - \lambda \cdot p}{1 - \lambda}, \forall p \in P \mid \lambda \in [0; 1], \lambda \cdot p \leq \overline{p} \right\} \\ &= \{ p_r, \forall p_r \in P \mid \lambda \in [0; 1], (1 - \lambda) \cdot p_r \leq \overline{p} \} \end{aligned}$$

$$\begin{aligned} P_2 &= \left\{ p_r = \tfrac{\overline{p} - (1 - \lambda) \cdot p}{\lambda}, \forall p \in P \mid \lambda \in [0; 1], (1 - \lambda) \cdot p \leq \overline{p} \right\} \\ &= \{ p_r, \forall p_r \in P \mid \lambda \in [0; 1], \lambda \cdot p_r \leq \overline{p} \} \end{aligned}$$

Without further assumptions on p_2 (without a prior on its probability distribution), we only know that $p(p_1 | p_+ = \overline{p}) = p(p_1 | p_1 \in P_1)$ and $p(p_2 | p_+ = \overline{p}_\alpha) = p(p_1 = \overline{p}_\alpha - \lambda_\alpha \cdot p_2 | p_2 \in P_2)$.[2]

Lemma 2. ***Extreme mixtures lemma.*** *Consider two independent arbitrary probability distributions p_1 and p_2. Given only a third probability distribution $p_+ = \overline{p}$ composed of the weighted mixture of the two, and for a small $\lambda \approx 0$, we can find a small residual hyperplane P_1, which tends to $\{\overline{p}\}$.*

$$P_1 \approx \{ p_r = \overline{p} - \lambda \cdot p, \forall p \in P \mid \lambda \cdot p \leq \overline{p} \} \quad \lambda \approx 0 \tag{4}$$

We can also find a very large residual hyperplane P_2 for p_2, which tends to:

$$\lim_{\lambda \to 0} P_2 = \{ p, \forall p \in P \mid supp(p) \subseteq supp(\overline{p}) \} \tag{5}$$

Theorem 3. ***No free anomaly theorem.*** *Consider two independent arbitrary probability distributions p_{normal} and p_{anom}. For a small number of anomalies $\lambda \approx 0$, $p_{full} = \overline{p}$ gives us no further knowledge on the distribution of p_{anom}:*

$$p(p_{anom} | p_{full} = \overline{p}) \approx Uniform(P_2), \quad \lambda \approx 0$$

From Theorem 3 we can conclude that, without a prior on the anomalies distribution, unsupervised anomaly detection is an undecidable problem. A more tangible example of this can be seen in Figure 1, where we present a synthetic data distribution composed of three classes of data clustered in four visibly separable clusters. Anomaly detection is a mainly undecidable problem in this setting without further information, since its impossible to decide if the low density cluster is composed of anomalies or the anomalies are the unclustered low density points (or a combination of both).

If we used a high capacity model to model the data distribution in Figure 1, the low density points (Right) would probably be detected as anomalous. If we used a low capacity model, the cluster (Center) would probably present a higher anomaly score. In real settings, network invasion attacks (anomalies) are usually clustered data points, while health insurance frauds can be either clustered or scattered (low density) points. In clinical data, some low density clusters may indicate diseases (anomalies), while other low density clusters may be caused by uncontrolled factors in the data, such as high performance athletes, for example. We want to be able to distinguish between anomalies and 'uninteresting' low probability points.

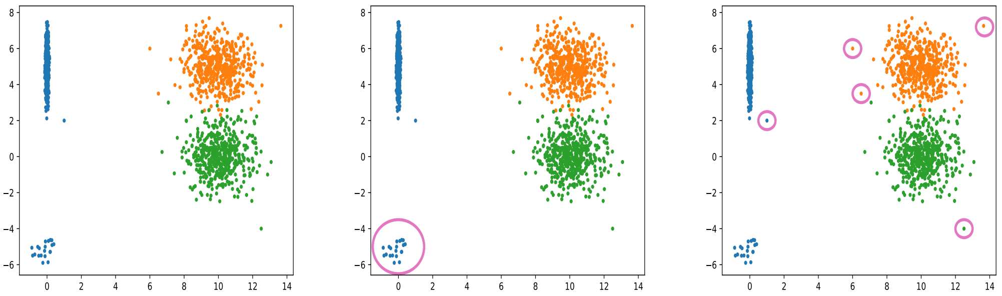

Figure 1: Example of undecidable anomalous data distribution: (Left) Raw data distribution; (Center) Possible Clustered Anomalies; (Right) Possible Low Density Anomalies.

[2] The proofs for all lemmas and theorems presented here can be found in Appendix D

3 Model

The usual strategy for solving unsupervised anomaly detection problems is training a parameterized model $p_\theta(x)$ to capture the full data distribution $p_{full}(x)$ (e.g. a PCA, or AutoEncoder), and, since λ is, by definition, a small constant, assuming $p_{full}(x) \approx p_{normal}(x)$ and assuming points with low probability are anomalous [Zhou and Paffenroth, 2017]. An anomaly score $s(x)$ is then defined as $s(x) = \frac{1}{p(x)}$. There are three main problems with this strategy:

1. if anomalous items are more common than desired, p_{full} might be a poor approximation of p_{normal};
2. if anomalous items are tightly clustered in some way, high capacity models may learn to identify that cluster as a high probability region;
3. since we only have access to p_{full}, Theorem 3 states that its impossible to recover the separate distributions p_{normal} and p_{anom} without further information/assumptions on their probability distributions.

Most unsupervised anomaly detection systems also rely on further verification of the results by human experts, due to their uncertain performance. Being mostly used as a ranking system to get high probability instances in the top of a ‘list’ to be further audited by these experts.

From Theorem 3, we conclude it is impossible to have an universal and reliable unsupervised anomaly detection system, while we know that most such systems already rely on the data being later audited by human experts. These arguments together argue in favor of an active learning strategy for anomaly detection, including the auditor experts in the system’s training loop. Thus, anticipating feedback and benefiting from it to find further anomalous instances, which results in a more robust system.

Having an extremely unbalanced dataset in this problem ($\lambda \approx 0$) is also another justification for an active learning setting, which has the potential of requiring exponentially less labeled data than supervised settings [Settles, 2012].

3.1 Active Anomaly Detection

With these motivations, we argue in favor of the new category of anomaly detection algorithms called *active anomaly detection*. In unsupervised anomaly detection we start with a dataset $\mathcal{D} = \{x | x \sim p_{full}(x)\}$ and want to rank elements in this dataset so that we have the highest possible recall/precision for a certain budget b, which is the number of elements selected to be audited by an expert, with no prior information on anomaly labels.

In active anomaly detection, we also start with a completely unlabeled anomaly detection dataset $\mathcal{D} = \{x | x \sim p_{full}(x)\}$, but instead of ranking anomalies and sending them all to be audited at once by our expert, we select them in small parts, waiting for the experts feedback before continuing. We iteratively select the most probable $k \ll b$ elements to be audited, wait for the expert to select their label, and continue training our system using this information, as shown in Algorithm 1. This requires the same budget b as an unsupervised anomaly detection system, while having the potential of achieving a much better performance.

Algorithm 1 Active Anomaly Detection

```
procedure ActiveAnomalyDetection($\mathcal{D}$, expert, $b$, $k$)
    $i \leftarrow 0$
    $labels \leftarrow \emptyset$
    while $i < b$ do
        $model$.train($\mathcal{D}, labels$)
        $top\_k \leftarrow model$.select_top($k, \mathcal{D}, labels$)
        $labels \leftarrow labels \cup expert$.audit($top\_k$)
        $i \leftarrow i + k$
```

With this in mind, we develop the Universal Anomaly Inference (UAI) layer. This layer can be incorporated on top of any deep learning based white box anomaly detection system which provides an anomaly score for ranking anomalies. It takes as input both a latent representation layer ($l(x)$), created by the model, and its output anomaly score ($s(x)$), and passes it through a classifier to find an item's anomaly probability.

$$s_{uai}(x) = p_{anom}(x) = \mathit{classifier}([l(x); s(x)]) \tag{6}$$

This is motivated by recent works stating learned representations have a simpler statistical structure [Bengio et al., 2013], which makes the task of modeling this manifold and detecting unnatural points much simpler [Lamb et al., 2018]. In this work, we model the UAI layer using a simple logistic regression as our classifier, but any architecture could be used here:

$$s_{uai}(x) = p_{anom}(x) = \sigma(W_{act}[l(x); s(x)] + b_{act}) \tag{7}$$

where $W_{act} \in \mathbb{R}^{1,d+1}$ is a linear transformation, $b_{act} \in \mathbb{R}$ is a bias term and $\sigma(\cdot)$ is the sigmoid function. We learn the values of W and b using back-propagation with a cross entropy loss function, while allowing the gradients to flow through l, but not through s, since s might be non-differentiable. For the rest of this document, we will refer to the networks with a UAI layer as UaiNets.

4 Experiments

In this section, we test our new UAI layer on top of two distinct architectures: a Denoising AutoEncoder (DAE, with $s_{dae}(x) = ||x - \hat{x}||_2^2$) and a Classifier ($Class$, with $s_{class}(x) = cross\_entropy(x_y, \widehat{x_y})$), which use standard multi layer perceptrons. Both architectures are described in details in Appendix A.1. To test our algorithm we start by analyzing its performance on synthetic datasets with very different properties, presented in Section 4.1. We then present results using UaiNets on real anomaly detection datasets, shown in Section 4.2.

4.1 Synthetic Data

When designing experiments, we had the objective of showing that our model can work with different definitions of anomaly, while completely unsupervised models will need, by definition, to trade-off accuracy in one setting for accuracy in the other. With this in mind, we used the MNIST dataset and defined four sets of experiments:[3]

1. **MNIST$_\mathbf{0}$**: For the first set of experiments, we reduced the presence of the 0 digit class to only 10% of its original number of samples, making it only $1/91 \approx 1.1\%$ of the dataset samples. The 0s still present in the dataset had its class randomly changed to $x_y \sim \mathit{Uniform}([1; 9])$ and were defined as anomalies.
2. **MNIST$_\mathbf{0\text{-}2}$**: The second set of experiments follows the same dataset construction, but we reduce the number of instances of numbers 0, 1 and 2, changing the labels of the remaining items in these categories to $x_y \sim \mathit{Uniform}([3; 9])$, and again defining them as anomalous. In this dataset anomalies composed $3/73 \approx 4.1\%$ of the dataset.
3. **MNIST$_\mathbf{hard}$**: The third set of experiments aims to test a different type of anomaly. In order to create this dataset, we first trained a weak one hidden layer MLP classifier on MNIST and selected all misclassified instances as anomalous, keeping them in the dataset with their original properties (x_x and x_y). In this dataset anomalies composed $\approx 3.3\%$ of the dataset.
4. **MNIST$_\mathbf{pca}$**: In this set of experiments, for each image class (x_y), we used a PCA to reduce the dimensionality of MNIST images (x_x) to 2 and selected the 5% instances with the largest reconstruction error as anomalies. We kept all $60{,}000$ instances in the dataset with their original properties (x_x and x_y) and in this dataset anomalies composed 5% of the dataset.

Figure 2(a) presents results for MNIST$_0$. On this dataset, we can see that $Class$ has similar results to $Class_{uai}$ only for the first 100 items selected, with $Class_{uai}$ having already selected almost all 600 anomalies in this dataset with a budget $b = 1{,}000$, while $Class$ plateaus after selecting around 450 anomalies and has difficulty finding the last one hundred ones.[4] Analogously, DAE produces similar

[3] Implementation details, such as the used architecture and hyper-parameters can be found in Appendix A, as well as further details about the synthetic MNIST datasets. Using MNIST for the generation of synthetic anomaly detection datasets follows recent works [Zhai et al., 2016, Zhou and Paffenroth, 2017].

[4] Due to lack of space we only report full results here, but the same plots zoomed in for small budgets ($b \leq 5000$) can be found in Appendix B.1.

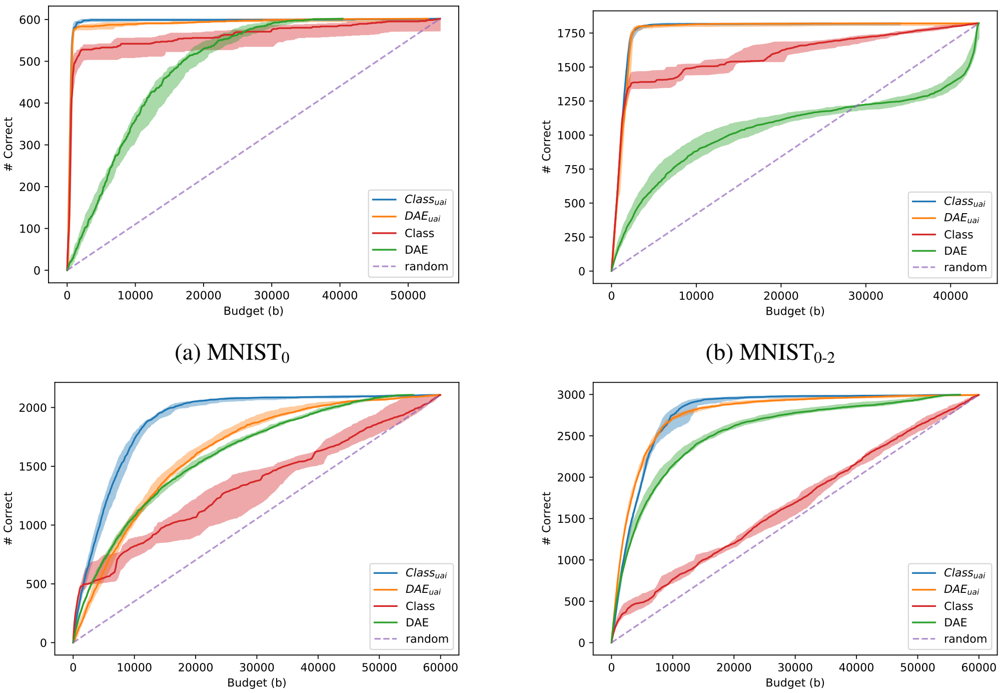

(a) MNIST$_0$

(b) MNIST$_{0\text{-}2}$

(c) MNIST$_{\text{hard}}$

(d) MNIST$_{\text{pca}}$

Figure 2: (Color online) Results for different MNIST experiments. Lines represent median of five runs with different seeds and confidence intervals represent max and min results for each budget b.

results to DAE_{uai} for a budget of up to $b = 100$ (when DAE_{uai} is actually using DAE to select items), but after this cold start period DAE_{uai} even outperforms $Class$, which does much better than DAE, achieving a performance close to perfect together with $Class_{uai}$.

In Figure 2(b) we see similar trends on MNIST$_{0\text{-}2}$, where the DAE model has so much difficulty to select the last items that it actually does worse than random. This further supports our claim that high capacity models can overfit to some anomalous clusters, not being able to identify them as anomalous. DAE_{uai}, on the contrary, can easily identify them and has a similar or better performance than $Class$ for large budgets.

Figure 2(c) presents results for the harder task of identifying the different anomalies present in MNIST$_{\text{hard}}$. On this dataset we see all algorithms have more difficulty finding anomalies, with DAE and $Class$ outperforming DAE_{uai} and $Class_{uai}$ for budgets $b < 1{,}500$ and $b < 10{,}000$ respectively. We also see that, after this hot start, $Class$ actually becomes the worst between the four methods, having a hard time in finding more than 600 of the approximately 2,000 anomalies. At the same time, after their cold start, DAE_{uai} and $Class_{uai}$ fare well on this task, with $Class_{uai}$ having clearly the best results on this task.

Finally, the results for the task of identifying anomalies present in MNIST$_{\text{pca}}$ are presented in Figure 2(d). On this dataset we clearly see that DAE_{uai} and $Class_{uai}$ fare substantially better than their underlining models DAE and $Class$.

The main conclusion from these experiments is that, even though our algorithm might not get better results than its underlying model for every budget-dataset pair, it is robust to different types of anomalies, which is not the case for the underlying completely unsupervised models. While $Class$ gives really good results in MNIST$_0$ and MNIST$_{0\text{-}2}$ datasets, it does not achieve the same performance in MNIST$_{\text{hard}}$ and MNIST$_{\text{pca}}$, which might indicate it is better at finding clustered anomalies than low density ones. At the same time, DAE has really good results for MNIST$_{\text{pca}}$, acceptable results for MNIST$_{\text{hard}}$, and bad ones for MNIST$_0$ and MNIST$_{0\text{-}2}$, which indicates it is better at finding low density anomalies than clustered ones. Nevertheless, both UaiNets are robust in all four datasets, being able to learn even on datasets which are hard for their underlying models, although they might have a colder start to produce results.[5]

4.2 Real Data

Here we analyze our model's performance on public benchmarks composed of real anomaly detection datasets. We employ four datasets in our analysis: KDDCUP [Lichman, 2013]; Thyroid [Lichman, 2013]; Arrhythmia [Lichman, 2013]; and KDDCUP-Rev [Lichman, 2013]. We use them in the same manner as described in [Zong et al., 2018] and further statistics on the datasets can be seen in Table 1. We compare our algorithm against: OC-SVM [Chen et al., 2001]; DAE [Vincent et al., 2008]; DCN [Yang et al., 2017]; DAGMM [Zong et al., 2018]; and LODA-AAD [Das et al., 2016].[6]

Table 1: Real Datasets Statistics

	# Dimensions	# Instances	# Anomalies	Anomaly Ratio
KDDCUP	120	494,021	97,278	20%
Thyroid	6	3,772	93	2.5%
Arrhythmia	274	452	66	15%
KDDCUP-Rev	120	121,597	24,319	20%

Table 2 presents results for these real datasets. In these experiments, OC-SVM, DCN and DAGMM were trained on a semi-supervised anomaly detection setting, using clean/cleaner datasets during training, DAE was trained in an unsupervised setting, while LODA-AAD and DAE_{uai} were trained in an active anomaly detection setting. We can clearly see from these results that DAE produces fairly bad results for all datasets analyzed here, nevertheless, even using a simple architecture as its underlying model, DAE_{uai} produces similar results to the best baselines on the four datasets, even when the baselines were trained in completely clean training sets. DAE_{uai} also presents better results than LODA-AAD, which is similarly trained in an active anomaly detection setting.

Table 2: Results on Real Datasets showing mean of five independent runs.[7]

	KDDCUP				Arrhythmia			
	Train Set λ	Precision	Recall	F1	Train Set λ	Precision	Recall	F1
OC-SVM	0%	0.75	0.85	0.80	0%	**0.54**	0.41	0.46
DCN	0%	0.77	0.78	0.78	0%	0.38	0.39	0.38
DAGMM	0%	0.93	**0.94**	**0.94**	0%	0.49	**0.51**	**0.50**
DAGMM*	0%	0.93	**0.94**	**0.94**	0%	0.49	**0.51**	**0.50**
DAGMM*	5%	0.88	0.89	0.89	3%	0.45	0.47	0.46
DAGMM*	20%	0.42	0.43	0.43	15%	0.45	0.46	0.46
LODA-AAD	20%	0.88	0.88	0.88	15%	0.45	0.45	0.45
DAE	20%	0.39	0.39	0.39	15%	0.35	0.35	0.35
DAE_{uai}	20%	**0.94**	**0.94**	**0.94**	15%	**0.47**	**0.47**	**0.47**

	Thyroid				KDDCUP-Rev			
	Train Set λ	Precision	Recall	F1	Train Set λ	Precision	Recall	F1
OC-SVM	0%	0.36	0.42	0.39	0%	0.71	**0.99**	0.83
DCN	0%	0.33	0.32	0.33	0%	0.29	0.29	0.29
DAGMM	0%	0.48	0.48	0.48	0%	**0.94**	0.94	**0.94**
DAGMM*	0%	0.44	0.45	0.44	0%	**0.94**	0.94	**0.94**
DAGMM*	0.5%	0.29	0.29	0.29	5%	0.32	0.36	0.33
DAGMM*	2.5%	0.45	0.46	0.46	20%	0.31	0.31	0.31
LODA-AAD	2.5%	0.51	0.51	0.51	20%	0.83	0.83	0.83
DAE	2.5%	0.09	0.09	0.09	20%	0.16	0.16	0.16
DAE_{uai}	2.5%	**0.57**	**0.57**	**0.57**	20%	**0.91**	**0.91**	**0.91**

[5] We also report the same experiments with similar results on Appendix B.3 for the MNIST-Fashion dataset.

[6] Further descriptions of these datasets and baselines can be found in Appendix A.3, as well as descriptions of the used architectures and hyper-parameters.

[7] Results for OC-SVM, DSEBM-e, DCN and DAGMM were taken from [Zong et al., 2018], while DAGMM* are results from our implementation of DAGMM. Unfortunately, we were not able to reproduce their results in Thyroid. For more detailed results, standard deviations and comparison to other baselines see Appendix B.2

5 Related Works

Anomaly Detection This field has been amply studied and good overviews can be found in [Chandola et al., 2009, Hodge and Austin, 2004]. Although many algorithms have been recently proposed, classical methods for outlier detection, like LOF Breunig et al. [2000] and OC-SVM [Schölkopf et al., 2001], are still used and produce good results. Recent work on anomaly detection has focused on statistical properties of "normal" data to identify these anomalies, such as Maurus and Plant [2017], which uses Benford's Law to identify anomalies in social networks, and [Siffer et al., 2017], which uses Extreme Value Theory to detect anomalies. Other works focus on specific types of data, [Zheng et al., 2017] focuses on spatially contextualized data, while [Li et al., 2017, Liu et al., 2017, Perozzi and Akoglu, 2016, Perozzi et al., 2014] focus on graph data. Recently, energy based models [Zhai et al., 2016] and GANs [Schlegl et al., 2017] have been successfully used to detect anomalies, but autoencoders are still more popular in this field. Zhou and Paffenroth [2017] propose a method to train robust autoencoders, drawing inspiration from robust statistics [Huber, 2011] and more specifically robust PCAs, [Yang et al., 2017] focuses on clustering, and trains autoencoders that generate latent representations which are friendly for k-means. The work most similar to ours is DAGMM [Zong et al., 2018], where they train a deep autoencoder and use its latent representations, together with its reconstruction error, as input to a second network, which they use to predict the membership of each data instance to a mixture of gaussian models, training the whole model end-to-end in an semi-supervised manner for novelty detection.

Active Anomaly Detection In [Pelleg and Moore, 2005], the authors solve the rare-category detection problem by proposing an active learning strategy to datasets with extremely skewed distributions of class sizes. Abe et al. [2006] reduces outlier detection to classification using artificially generated examples that play the role of potential outliers and then applies a selective sampling mechanism based on active learning to the reduced classification problem. In [Görnitz et al., 2013], the authors proposed a Semi-Supervised Anomaly Detection (SSAD) method based in Support Vector Data Description (SVDD) [Tax and Duin, 2004], which he expanded to a semi-supervised setting, where he accounts for the presence of labels for some anomalous instances, and with an active learning approach to select these instances to label. The most similar prior work to ours in this setting is [Das et al., 2016], which first describes Active Anomaly Detection (AAD) as a general approach to this problem and proposes an algorithm that can be employed with any ensemble methods based on random projections. Our work differs from these prior works mainly in that we show unsupervised anomaly detection is an undecidable problem and further formalize and motivate the proposed Active Anomaly Detection framework, contextualizing it with other anomaly detection settings. Our work also differs from them in our proposed model, which can be assembled on top of any anomaly detection Deep Learning architecture to make it work in an active anomaly detection setting.

6 Discussions and Future Work

We proposed here a new architecture, Universal Anomaly Inference (UAI), which can be applied on top of any deep learning based anomaly detection architecture. We show that, even on top of very simple architectures, like a DAE, UaiNets can produce similar/better results to state-of-the-art unsupervised/semi-supervised anomaly detection methods.

We further want to make clear that we are not stating our method is better than any of our baselines (DAGMM, DCN, DSEBM-e, or OC-SVM) and our contributions are orthogonal to theirs. We are proposing a new approach to this hard problem which can be built on top of them, this being our main contribution in this work. We formalized *active anomaly detection* as an approach to unsupervised anomaly detection, giving both theoretical and practical arguments in favor of it, arguing that, in most practical settings, there would be no detriment to using this instead of a fully unsupervised approach.

Important future directions for this work are using the UAI layers confidence in its output to dynamically choose between either directly using its scores, or using the underlying unsupervised model's anomaly score to choose which instances to audit next. Another future direction would be testing new architectures for UAI layers, in this work we restricted all our analysis to simple logistic regression UAI layers. A third important future work would be analyzing the robustness of UaiNets to mistakes being made by the labeling experts. Finally, making this model more interpretable, so that auditors could focus on a few "important" features when labeling anomalous instances, could increase labeling speed and make their work easier.

References

Martín Abadi, Paul Barham, Jianmin Chen, Zhifeng Chen, Andy Davis, Jeffrey Dean, Matthieu Devin, Sanjay Ghemawat, Geoffrey Irving, Michael Isard, Manjunath Kudlur, Josh Levenberg, Rajat Monga, Sherry Moore, Derek Gordon Murray, Benoit Steiner, Paul A. Tucker, Vijay Vasudevan, Pete Warden, Martin Wicke, Yuan Yu, and Xiaoqiang Zheng. Tensorflow: A system for large-scale machine learning. In *OSDI*, volume 16, pages 265–283, 2016.

Naoki Abe, Bianca Zadrozny, and John Langford. Outlier detection by active learning. In *Proceedings of the 12th ACM SIGKDD international conference on Knowledge discovery and data mining*, pages 504–509. ACM, 2006.

Charu C Aggarwal. Outlier analysis. In *Data mining*, pages 237–263. Springer, 2015.

Yoshua Bengio, Grégoire Mesnil, Yann Dauphin, and Salah Rifai. Better mixing via deep representations. In *International Conference on Machine Learning*, pages 552–560, 2013.

Markus M Breunig, Hans-Peter Kriegel, Raymond T Ng, and Jörg Sander. Lof: identifying density-based local outliers. In *ACM sigmod record*, volume 29, pages 93–104. ACM, 2000.

Varun Chandola, Arindam Banerjee, and Vipin Kumar. Anomaly detection: A survey. *ACM computing surveys (CSUR)*, 41(3):15, 2009.

Yunqiang Chen, Xiang Sean Zhou, and Thomas S Huang. One-class svm for learning in image retrieval. In *Image Processing, 2001. Proceedings. 2001 International Conference on*, volume 1, pages 34–37. IEEE, 2001.

Shubhomoy Das, Weng-Keen Wong, Thomas Dietterich, Alan Fern, and Andrew Emmott. Incorporating expert feedback into active anomaly discovery. In *International Conference on Data Mining (ICDM)*, pages 853–858. IEEE, 2016.

Anirban Dasgupta, John Hopcroft, Jon Kleinberg, and Mark Sandler. On learning mixtures of heavy-tailed distributions. In *Foundations of Computer Science, 2005. FOCS 2005. 46th Annual IEEE Symposium on*, pages 491–500. IEEE, 2005.

Nico Görnitz, Marius Kloft, Konrad Rieck, and Ulf Brefeld. Toward supervised anomaly detection. *Journal of Artificial Intelligence Research*, 46:235–262, 2013.

Frank E Grubbs. Procedures for detecting outlying observations in samples. *Technometrics*, 11(1): 1–21, 1969.

Douglas M Hawkins. *Identification of outliers*, volume 11. Springer, 1980.

Victoria Hodge and Jim Austin. A survey of outlier detection methodologies. *Artificial intelligence review*, 22(2):85–126, 2004.

Peter J Huber. Robust statistics. In *International Encyclopedia of Statistical Science*, pages 1248–1251. Springer, 2011.

Alex Lamb, Jonathan Binas, Anirudh Goyal, Dmitriy Serdyuk, Sandeep Subramanian, Ioannis Mitliagkas, and Yoshua Bengio. Fortified networks: Improving the robustness of deep networks by modeling the manifold of hidden representations. *arXiv preprint arXiv:1804.02485*, 2018.

Yann LeCun, Sumit Chopra, Raia Hadsell, M Ranzato, and F Huang. A tutorial on energy-based learning. *Predicting structured data*, 1(0), 2006.

Jundong Li, Harsh Dani, Xia Hu, and Huan Liu. Radar: Residual analysis for anomaly detection in attributed networks. In *Proceedings of the 26th International Joint Conference on Artificial Intelligence*, pages 2152–2158. AAAI Press, 2017.

Moshe Lichman. Uci machine learning repository, 2013.

Ninghao Liu, Xiao Huang, and Xia Hu. Accelerated local anomaly detection via resolving attributed networks. In *Proceedings of the 26th International Joint Conference on Artificial Intelligence*, pages 2337–2343. AAAI Press, 2017.

Samuel Maurus and Claudia Plant. Let's see your digits: Anomalous-state detection using benford's law. In *Proceedings of the 23rd ACM SIGKDD International Conference on Knowledge Discovery and Data Mining*, pages 977–986. ACM, 2017.

Dan Pelleg and Andrew W Moore. Active learning for anomaly and rare-category detection. In *Advances in neural information processing systems*, pages 1073–1080, 2005.

Bryan Perozzi and Leman Akoglu. Scalable anomaly ranking of attributed neighborhoods. In *Proceedings of the 2016 SIAM International Conference on Data Mining*, pages 207–215. SIAM, 2016.

Bryan Perozzi, Leman Akoglu, Patricia Iglesias Sánchez, and Emmanuel Müller. Focused clustering and outlier detection in large attributed graphs. In *Proceedings of the 20th ACM SIGKDD international conference on Knowledge discovery and data mining*, pages 1346–1355. ACM, 2014.

Tomáš Pevnỳ. Loda: Lightweight on-line detector of anomalies. *Machine Learning*, 102(2):275–304, 2016.

Thomas Schlegl, Philipp Seeböck, Sebastian M Waldstein, Ursula Schmidt-Erfurth, and Georg Langs. Unsupervised anomaly detection with generative adversarial networks to guide marker discovery. In *International Conference on Information Processing in Medical Imaging*, pages 146–157. Springer, 2017.

Bernhard Schölkopf, John C Platt, John Shawe-Taylor, Alex J Smola, and Robert C Williamson. Estimating the support of a high-dimensional distribution. *Neural computation*, 13(7):1443–1471, 2001.

Burr Settles. Active learning. *Synthesis Lectures on Artificial Intelligence and Machine Learning*, 6 (1):1–114, 2012.

Alban Siffer, Pierre-Alain Fouque, Alexandre Termier, and Christine Largouet. Anomaly detection in streams with extreme value theory. In *Proceedings of the 23rd ACM SIGKDD International Conference on Knowledge Discovery and Data Mining*, pages 1067–1075. ACM, 2017.

David MJ Tax and Robert PW Duin. Support vector data description. *Machine learning*, 54(1):45–66, 2004.

Pascal Vincent, Hugo Larochelle, Yoshua Bengio, and Pierre-Antoine Manzagol. Extracting and composing robust features with denoising autoencoders. In *International Conference on Machine learning*, pages 1096–1103. ACM, 2008.

Pascal Vincent, Hugo Larochelle, Isabelle Lajoie, Yoshua Bengio, and Pierre-Antoine Manzagol. Stacked denoising autoencoders: Learning useful representations in a deep network with a local denoising criterion. *Journal of Machine Learning Research*, 11(Dec):3371–3408, 2010.

Han Xiao, Kashif Rasul, and Roland Vollgraf. Fashion-mnist: a novel image dataset for benchmarking machine learning algorithms, 2017.

Bo Yang, Xiao Fu, Nicholas D Sidiropoulos, and Mingyi Hong. Towards k-means-friendly spaces: Simultaneous deep learning and clustering. In *International Conference on Machine Learning*, pages 3861–3870, 2017.

Shuangfei Zhai, Yu Cheng, Weining Lu, and Zhongfei Zhang. Deep structured energy based models for anomaly detection. *arXiv preprint arXiv:1605.07717*, 2016.

Guanjie Zheng, Susan L Brantley, Thomas Lauvaux, and Zhenhui Li. Contextual spatial outlier detection with metric learning. In *Proceedings of the 23rd ACM SIGKDD International Conference on Knowledge Discovery and Data Mining*, pages 2161–2170. ACM, 2017.

Chong Zhou and Randy C Paffenroth. Anomaly detection with robust deep autoencoders. In *Proceedings of the 23rd ACM SIGKDD International Conference on Knowledge Discovery and Data Mining*, pages 665–674. ACM, 2017.

Bo Zong, Qi Song, Martin Renqiang Min, Wei Cheng, Cristian Lumezanu, Daeki Cho, and Haifeng Chen. Deep autoencoding gaussian mixture model for unsupervised anomaly detection. In *International Conference on Learning Representations*, 2018.

A Experiments Descriptions

In this section we give detailed descriptions of the experiments. Section A.1 presents the used model architectures for both DAE and $Class$ models, as well as DAE_{uai} and $Class_{uai}$. Section A.2 presents details on the synthetic MNIST datasets and on the hyper-parameters used for the experiments. Finally, Section A.3 contains detailed descriptions on the used datasets, baselines and experimental settings for the experiments on real anomaly detection datasets.

A.1 Model Architectures

To show our algorithm can be assembled on top of any deep learning model, we tested it using two simple but very different anomaly detection models. The first model we test it on top of is a normal Denoising AutoEncoder (DAE).

A DAE is a neural network mainly composed by an encoder, which transforms the input into a latent space, and a decoder, which reconstructs the input using this latent representation, typically having a loss function that minimizes the reconstruction error L_2 norm:

$$\begin{aligned} l &= f_{enc}(x+\epsilon) \quad \epsilon \sim \mathcal{N}(0,\varphi) \\ \hat{x} &= f_{dec}(l) \\ \mathcal{L} &= ||x-\hat{x}||_2^2 \end{aligned} \tag{8}$$

where both f_{enc} and f_{dec} are usually feed forward networks with the same number of layers, $l \in \mathbb{R}^d$ is a d-dimensional latent representation and ϵ is a zero mean noise, sampled from a Gaussian distribution with a φ standard deviation. When used in anomaly detection, the reconstruction error is usually used as an approximation of the inverse of an item's probability, and as its anomaly score:

$$s_{dae}(x) = \frac{1}{p(x)} = ||x-\hat{x}||_2^2 \tag{9}$$

We then create a DAE_{uai} network by assembling the proposed UAI layer on top of the DAE:

$$\begin{aligned} l_{dae} &= l = f_{enc}(x+\epsilon) \\ s_{dae-uai}(x) &= uai([l_{dae}; s_{dae}]) \end{aligned} \tag{10}$$

where $uai(\cdot)$ is the classifier chosen for the UAI layer. Another typical approach to unsupervised anomaly detection is, when given a dataset with labeled data $X = (x_x, x_y)$, training a classifier ($Class$) to predict x_y from x_x[8] and using the cross-entropy of an item as an approximation to the inverse of its probability distribution:

$$\begin{aligned} \widehat{x_y} &= f_{class}(x) \\ \mathcal{L} &= cross\_entropy(x_y, \widehat{x_y}) \\ s_{class}(x) &= \tfrac{1}{p(x)} = cross\_entropy(x_y, \widehat{x_y}) \end{aligned} \tag{11}$$

where $f_{class}(\cdot)$ is typically a feed forward neural network with p layers, from which we can use its last hidden layer (h_{p-1}) as the data's latent representation to be used in the $Class_{uai}$.

$$\begin{aligned} l_{class} &= h_{p-1} \\ s_{class-uai}(x) &= uai([l_{class}; s_{class}]) \end{aligned} \tag{12}$$

For all experiments in this work, unless otherwise stated, the DAE's encoder and decoder had independent weights and we used both the DAE and $Class$ models with 3 hidden layers and hidden sizes $[256, 64, 8]$. This means the latent representations provided to the UAI layers are $l \in \mathbb{R}^8$. We implemented all experiments using TensorFlow [Abadi et al., 2016], and used a learning rate of 0.01, batch size of 256 and the RMSprop optimizer with the default hyper-parameters. For the active learning models, we pre-train the DAE/Class model for 5000 optimization steps, select $k = 10$ items to be labeled at a time, and further train for 100 iterations after each labeling call. To deal with the cold start problem, for the first 10 calls of select_top, we use the base anomaly score (s) of the DAE/$Class$ model to make this selection, using the UAI one for all later labeling decisions.

[8] Note that, even though in this problem we have class labels (x_y), we have no anomaly labels of objects (y), so this is still an unsupervised anomaly detection problem.

Table 3: MNIST Anomaly Datasets Statistics

	# Dimensions	# Classes	# Instances	# Anomalies	Anomaly Ratio
MNIST_0	784	9	54,679	602	1.1%
$\text{MNIST}_{0\text{-}2}$	784	7	43,199	1,822	4.2%
$\text{MNIST}_{\text{hard}}$	784	10	60,000	2,108	3.5%
$\text{MNIST}_{\text{pca}}$	784	10	60,000	2,996	5%

A.2 Synthetic Data

Detailed statistics on the synthetic MNIST datasets can be seen in Table 3. MNIST_0 and $\text{MNIST}_{0\text{-}2}$ were mainly generated with the purpose of simulating the situation in Figure 1 (Center), where anomalies were present in sparse clusters. At the same time, $\text{MNIST}_{\text{hard}}$ and $\text{MNIST}_{\text{pca}}$ were designed to present similar characteristics to the situation in Figure 1 (Right), where anomalous instances are in sparse regions of the data space.

A.3 Real Data

For these experiments, we used the same datasets as [Zong et al., 2018] and preprocessed them in the same manner as them:

- **KDDCUP [Lichman, 2013]**: The KDDCUP99 10 percent dataset from the UCI repository. Since it contains only 20% of instances labeled as “normal” and the rest as “attacks”, “normal” instances are used as anomalies, since they are in a minority group. This dataset contains 34 continuous features and 7 categorical ones. We transform these 7 categorical features into their one hot representations, and obtain a dataset with 120 features.
- **Thyroid [Lichman, 2013]**: A dataset containing data from patients which can be divided in three classes: normal (not hypothyroid), hyperfunction and subnormal functioning. In this dataset, we treat the hyperfunction class as an anomaly, with the other two being treated as normal. It can be obtained from the ODDS repository.[9]
- **Arrhythmia [Lichman, 2013]**: This dataset was designed to create classification algorithms to distinguish between the presence and absence of cardiac arrhythmia. In it, we use the smallest classes (3, 4, 5, 7, 8, 9, 14, and 15) as anomalies and the others are treated as normal. This dataset can also be obtained from the ODDS repository.
- **KDDCUP-Rev [Lichman, 2013]**: Since “normal” instances are a minority in the KDDCUP dataset, we keep all “normal” instances and randomly draw “attack” instances so that they compose 20% of the dataset.

We compare our algorithm against:

- **OC-SVM** [Chen et al., 2001]: One-class support vector machines are a popular kernel based anomaly detection method. In this work, we employ it with a Radial Basis Function (RBF) kernel.
- **DAE** [Vincent et al., 2008]: Denoising Autoencoders are autoencoder architectures which are trained to reconstruct instances from noisy inputs.
- **DCN** [Yang et al., 2017]: Deep Clustering Network is a state-of-the-art clustering algorithm. Its architecture is designed to learn a latent representation using deep autoencoders which is easily separable when using k-means.
- **DAGMM** [Zong et al., 2018]: Deep Autoencoding Gaussian Mixture Model is a state-of-the-art model for semi-supervised anomaly detection which simultaneously learns a latent representation, using deep autoencoders, and uses both this latent representation and the autoencoder’s reconstruction error to learn a Gaussian Mixture Model for the data distribution.
- **LODA-AAD** [Das et al., 2016]: Lightweight on-line detector of anomalies (LODA) Active Anomaly Discovery (AAD) is a work which uses the active anomaly detection framework

[9] http://odds.cs.stonybrook.edu

on top of LODA [Pevnỳ, 2016], which is a method based on ensembles of weak anomaly detection models.

Since there is no validation/test set in unsupervised anomaly detection, we cannot tune hyperparameters on a validation set. Because of this, to make the DAE baselines more competitive, we got the results for several different hyper-parameter configurations and present only the best among them. This indeed is an unfair approach, but we only do it to our baselines, while for our proposed algorithm we keep hyper-parameters fixed for all experiments. We even keep our hidden sizes fixed to $[256, 64, 8]$ on thyroid, which only contains 6 features per instance, since our objective here is not getting the best possible results, but showing the robustness of our approach. The only hyper-parameter change we make in UAI networks is that, since there are fewer anomalies in Arrhythmia and Thyroid datasets, we set our active learning approach to choose 3 instances at a time, instead of 10.

Results for OC-SVM, DCN, and DAGMM were taken from [Zong et al., 2018], while results labeled as DAGMM* are from our implementation of this model and follow the same procedures as described in [Zong et al., 2018] and using the same architectures and hyper-parameters, being trained in a semi-supervised setting. The results for LODA-AAD were run using the code made available by the authors and with the same steps as DAE_{uai}.[10]

B Detailed Results

In this section, we present more detailed results for both the synthetic (Section B.1) and real (Section B.2) anomaly detection datasets, which couldn't fit on the main paper due to lack of space. We also present results for synthetic anomaly detection experiments on Fashion-MNIST (Section B.3).

B.1 Detailed Results on MNIST

We present here detailed results for small budgets ($b \leq 5000$) on the MNIST experiments, with graphs zoomed in for these budget values. Analyzing Figure 3 we see that for some of these datasets UaiNets present a cold start, producing worse results for small budgets. Nonetheless, after this cold start, they produce better results in all MNIST experiments. An interesting future work would be to measure the confidence in the UaiNet's prediction to dynamically choose between using its anomaly score or the underlying network's one, which could solve/reduce this cold start problem.

B.2 Detailed Results on Real Data

Table 4 presents detailed results for experiments on real datasets, showing standard deviations for the experiments we ran. In this table we also compare our results to:

- **PAE** [Vincent et al., 2008]: Denoising AutoEncoders pretrained as suggested in [Vincent et al., 2010].
- **DSEBM-e** [Zhai et al., 2016]: Deep Structured Energy Based Models are anomaly detection systems based on energy based models [LeCun et al., 2006], which are a powerful tool for density estimation. We compare here against DSEBM-e, which uses a data instance's energy as the criterion to detect anomalies.
- **DSEBM-r** [Zhai et al., 2016]: Deep Structured Energy Based Model with the same architecture and training procedures as DSEBM-e, but using an instance's reconstruction error as the criterion for anomaly detection.

The results presented here are averages of five runs, with standard deviations in parenthesis. In this table, results for OC-SVM, PAE, DSEBM-r, DSEBM-e, DCN and DAGMM were taken from [Zong et al., 2018], while DAGMM* are results from our implementation of DAGMM. Unfortunately, we were not able to reproduce their results in the Thyroid dataset, getting a high variance in the results. LODA-AAD does not scale well to large datasets, so to run it on KDDCUP and KDDCUP-Rev we needed to limit its memory about the anomalies it had already learned, forgetting the oldest ones.

[10] https://github.com/shubhomoydas/ad_examples

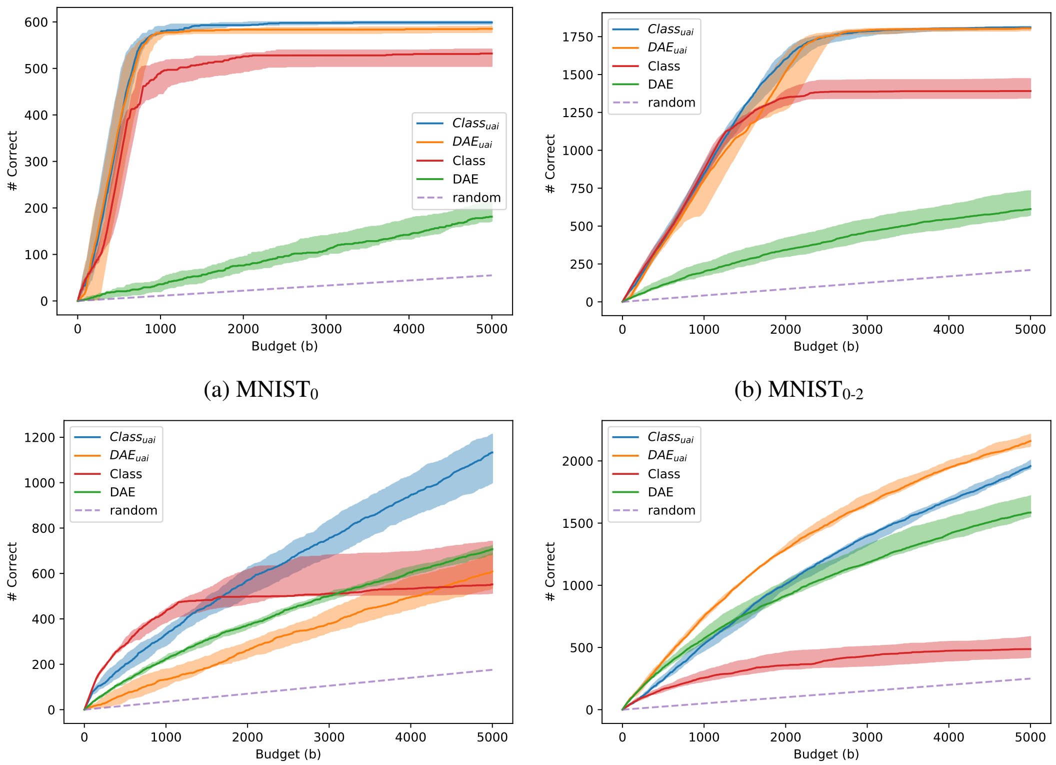

(a) MNIST$_0$

(b) MNIST$_{0\text{-}2}$

(c) MNIST$_{\text{hard}}$

(d) MNIST$_{\text{pca}}$

Figure 3: (Color online) Results for MNIST experiments zoomed in for $b \leq 5000$ on the x-axis. Lines represent median of five runs with different seeds and confidence intervals represent max and min results for each budget b.

This reduced its runtime complexity from $O(b^2)$ to $O(b)$ in our tests, where b is the budget limit for the anomaly detection task.

On this table we can see that DAE_{uai} produces better results than LODA-AAD on all analyzed datasets. Our proposed method also, besides presenting results comparable to state-of-the-art DAGMM trained on a clean dataset, is much more stable, having a lower standard deviation than the baselines in almost all datasets.

B.3 Experiments on Fashion-MNIST

In this Section, we present results for experiments on synthetic anomaly detection datasets based on Fashion-MNIST [Xiao et al., 2017]. To create these datasets we follow the same procedures as done for MNIST in Section 4.1, generating four datasets: Fashion-MNIST$_0$; Fashion-MNIST$_{0\text{-}2}$; Fashion-MNIST$_{\text{hard}}$; Fashion-MNIST$_{\text{pca}}$. Detailed statistics of these datasets can be seen in Table 5.

We run experiments on these datasets following the exact same procedures as in Section 4.1. Figure 4 shows the results for Fashion-MNIST$_0$ and Fashion-MNIST$_{0\text{-}2}$, while Figure 5 show the results for Fashion-MNIST$_{\text{hard}}$ and Fashion-MNIST$_{\text{pca}}$. These figures show similar trends to the ones for MNIST, although algorithms find anomalies in these datasets harder to identify. Specially for Fashion-MNIST$_{\text{hard}}$, $Class_{uai}$ takes a long time to start producing better results than $Class$. Nevertheless, UaiNets are still much more robust than the underlying networks to different types of anomalies, producing good results in all four datasets, even when its underlying network gives weak results on that dataset.

Table 4: Detailed results on real datasets showing mean and standard deviations of five runs.

Dataset	Method	Anomalies in Train Set	Precision	Recall	F1
KDDCUP	OC-SVM	0%	0.7457	0.8523	0.7954
	OC-SVM	5%	0.1155	0.3369	0.1720
	PAE	0%	0.7276	0.7397	0.7336
	DSEBM-r	0%	0.1972	0.2001	0.1987
	DSEBM-e	0%	0.7369	0.7477	0.7423
	DSEBM-e	5%	0.5345	0.5375	0.5360
	DCN	0%	0.7696	0.7829	0.7762
	DCN	5%	0.6763	0.6893	0.6827
	DAGMM	0%	0.9297	**0.9442**	0.9369
	DAGMM	5%	0.8504	0.8643	0.8573
	DAGMM*	0%	0.9290 (0.0344)	0.9435 (0.0349)	0.9362 (0.0346)
	DAGMM*	5%	0.8827 (0.0682)	0.8965 (0.0693)	0.8896 (0.0688)
	DAGMM*	20%	0.4238 (0.0187)	0.4304 (0.0190)	0.4271 (0.0188)
	LODA-AAD	20%	0.8756 (0.1255)	0.8756 (0.1255)	0.8756 (0.1255)
	DAE	20%	0.3905 (0.2581)	0.3905 (0.2581)	0.3905 (0.2581)
	DAE_{uai}	20%	**0.9401** (0.0191)	**0.9401** (0.0191)	**0.9401** (0.0191)
Thyroid	OC-SVM	0%	0.3639	0.4239	0.3887
	PAE	0%	0.1894	0.2062	0.1971
	DSEBM-r	0%	0.0404	0.0403	0.0403
	DSEBM-e	0%	0.1319	0.1319	0.1319
	DCN	0%	0.3319	0.3196	0.3251
	DAGMM	0%	0.4766	0.4834	0.4782
	DAGMM*	0%	0.4375 (0.1926)	0.4468 (0.1967)	0.4421 (0.1947)
	DAGMM*	0.5%	0.2875 (0.1505)	0.2936 (0.1537)	0.2905 (0.1521)
	DAGMM*	2.5%	0.4542 (0.2995)	0.4638 (0.3059)	0.4590 (0.3027)
	LODA-AAD	2.5%	0.5097 (0.0712)	0.5097 (0.0712)	0.5097 (0.0712)
	DAE	2.5%	0.0860 (0.0725)	0.0860 (0.0725)	0.0860 (0.0725)
	DAE_{uai}	2.5%	**0.5742** (0.0582)	**0.5742** (0.0582)	**0.5742** (0.0582)
Arrhythmia	OC-SVM	0%	**0.5397**	0.4082	0.4581
	PAE	0%	0.4393	0.4437	0.4403
	DSEBM-r	0%	0.1515	0.1513	0.1510
	DSEBM-e	0%	0.4667	0.4565	0.4601
	DCN	0%	0.3758	0.3907	0.3815
	GADMM	0%	0.4909	**0.5078**	**0.4983**
	GADMM*	0%	0.4902 (0.0514)	0.5051 (0.0530)	0.4975 (0.0522)
	GADMM*	3%	0.4530 (0.0573)	0.4666 (0.0591)	0.4597 (0.0582)
	GADMM*	15%	0.4500 (0.0597)	0.4636 (0.0615)	0.4567 (0.0606)
	LODA-AAD	15%	0.4485 (0.0136)	0.4485 (0.0136)	0.4485 (0.0136)
	DAE	15%	0.3485 (0.0392)	0.3485 (0.0392)	0.3485 (0.0392)
	DAE_{uai}	15%	**0.4727** (0.0225)	**0.4727** (0.0225)	**0.4727** (0.0225)
KDDCUP-Rev	OC-SVM	0%	0.7148	**0.9940**	0.8316
	PAE	0%	0.7835	0.7817	0.7826
	DSEBM-r	0%	0.2036	0.2036	0.2036
	DSEBM-e	0%	0.2212	0.2213	0.2213
	DCN	0%	0.2875	0.2895	0.2885
	GADMM	0%	0.9370	0.9390	0.9380
	GADMM*	0%	**0.9391** (0.1553)	0.9391 (0.1553)	**0.9391** (0.1553)
	GADMM*	5%	0.3184 (0.1358)	0.3559 (0.2096)	0.3341 (0.1658)
	GADMM*	20%	0.3051 (0.1059)	0.3053 (0.1060)	0.3052 (0.1059)
	LODA-AAD	20%	0.8339 (0.1081)	0.8339 (0.1081)	0.8339 (0.1081)
	DAE	20%	0.1626 (0.0609)	0.1626 (0.0609)	0.1626 (0.0609)
	DAE_{uai}	20%	**0.9117** (0.0160)	**0.9125** (0.0170)	**0.9121** (0.0165)

C Further Analysis

In this section we further study UaiNets, analyzing the evolution of hidden representations and anomaly scores through training (Section C.1), and the dependence of results on the number of audited anomalies (Section C.2).

C.1 Learned Representations and Anomaly Scores

In this section, we show visualizations of the learned representations ($l_{dae/class}$) and anomaly scores ($s_{dae/class}$) of UaiNets' underlying networks, presenting their evolution as more labels are fed into

Table 5: Fashion-MNIST Anomaly Datasets Statistics

	# Dimensions	# Classes	# Instances	# Anomalies	Anomaly Ratio
Fashion-MNIST$_0$	784	9	54,610	610	1.1%
Fashion-MNIST$_{0\text{-}2}$	784	7	43,765	1,765	4.0%
Fashion-MNIST$_{\text{hard}}$	784	10	60,000	9,656	16.1%
Fashion-MNIST$_{\text{pca}}$	784	10	60,000	3,000	5.0%

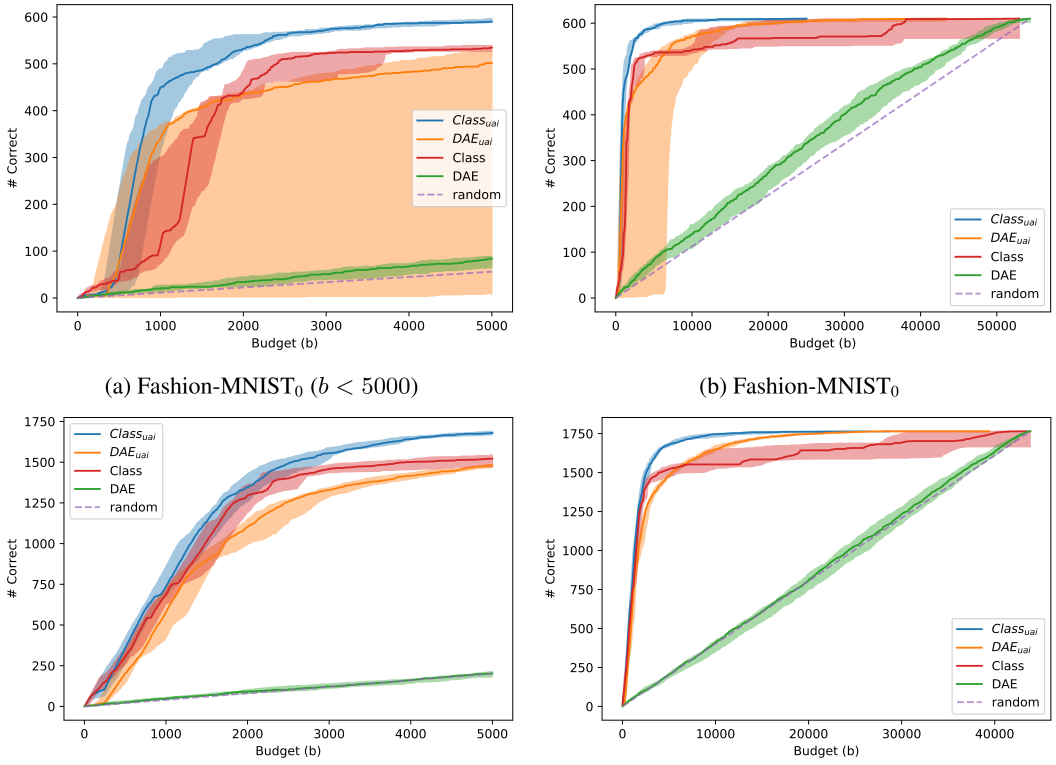

(a) Fashion-MNIST$_0$ ($b < 5000$)

(b) Fashion-MNIST$_0$

(c) Fashion-MNIST$_{0\text{-}2}$ ($b < 5000$)

(d) Fashion-MNIST$_{0\text{-}2}$

Figure 4: (Color online) Results for Fashion-MNIST$_0$ and Fashion-MNIST$_{0\text{-}2}$ with different zooms on x-axis. Lines represent median of five runs with different seeds and confidence intervals represent max and min results for each budget b.

the network through the active learning process. With this purpose, we retrain UaiNets on both MNIST$_{0\text{-}2}$ and MNIST$_{\text{hard}}$, with a hidden size of $[256, 64, 1]$, so that its latent representation is one dimensional ($l(x) \in R^1$), and plot these representations vs the anomaly scores (s) of the base network (either DAE or $Class$) for different budgets (b).

Figure 6 shows the evolution of DAE_{uai}'s underlying $l_{dae}(x)$ and $s_{dae}(x)$. In it, we can see that initially (Figures 6 (a, d)) anomalies and normal data instances are not separable in this space. Nevertheless, with only a few labeled instances ($b = 250$) the space becomes much easier to separate, while for $b = 2000$ the space is almost perfectly linearly separable.[11]

Figure 7 shows the same evolution for $Class_{uai}$'s underlying $l_{class}(x)$ and $s_{class}(x)$. In it, we can also see the same patterns, as initially anomalies and normal data instances are not separable, but with a few labeled instances anomalies become much more identifiable.

[11] Gifs showing these models evolution can be found in `https://homepages.dcc.ufmg.br/~tpimentel/paper_imgs/uai/hidden_vs_loss/`.

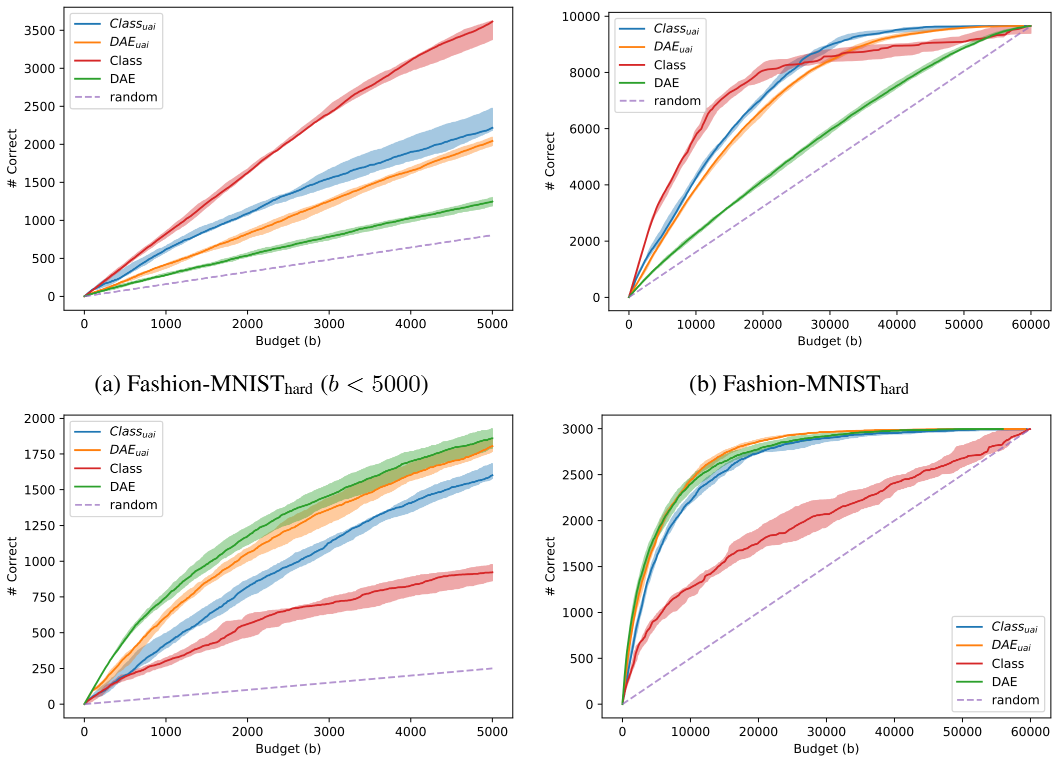

(a) Fashion-MNIST$_{\text{hard}}$ ($b < 5000$)

(b) Fashion-MNIST$_{\text{hard}}$

(c) Fashion-MNIST$_{\text{pca}}$ ($b < 5000$)

(d) Fashion-MNIST$_{\text{pca}}$

Figure 5: (Color online) Results for Fashion-MNIST$_{\text{hard}}$ and Fashion-MNIST$_{\text{pca}}$ with different zooms on x-axis. Lines represent median of five runs with different seeds and confidence intervals represent max and min results for each budget b.

The main conclusion taken from these visualizations is how the gradient flow through l is important, since it helps the network better separate data in these spaces, allowing good performance even when the underlying networks are not good at identifying a specific type of anomaly.

C.2 Anomaly Choices Evolution through Training

This experiments aim at showing how the networks choice quality evolves with the access to more labels. Here, we present the choices DAE_{uai} network would make having access to a fixed number of expert labels. With this in mind, we train the networks in the same way as in Section 4.2, but stop after reaching a specific budget (b), showing the choices made up to that point, and after that with no further training.

Figure 8 shows the evolution of DAE_{uai} anomaly choices as it is fed more expert knowledge. We can see that with only a few labels it already fairs a lot better than its underlying network. In KDDCUP with only $3{,}000$ labeled instances, which is less than 1% of the dataset, it can correctly find $80{,}000$ anomalies with a high precision, while the DAE with no expert knowledge does a lot worse. On Thyroid and KDDCUP-Rev, with $\approx 10\%$ of the dataset labeled ($b = 531$ and $b = 4000$, respectively) it finds all or almost all anomalies in the dataset correctly. The Arrhythmia dataset is a lot smaller and with few anomalies, so DAE_{uai} improves on DAE in a smaller scale here, but it still does fairly better than the underlying network.[12]

[12] Gifs showing this choice evolution can be found in `https://homepages.dcc.ufmg.br/~tpimentel/paper_imgs/uai/budget_evolution/`

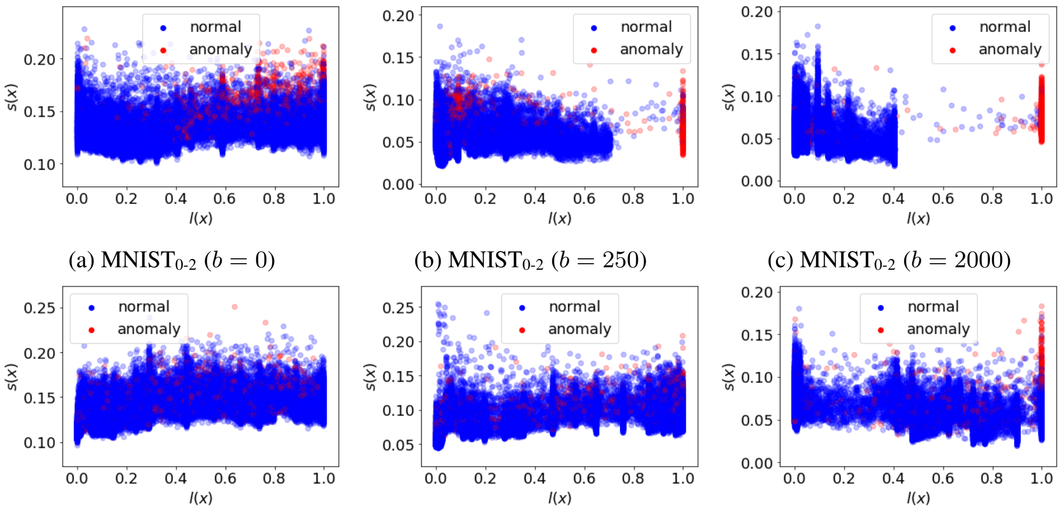

(a) MNIST$_{0\text{-}2}$ ($b = 0$)

(b) MNIST$_{0\text{-}2}$ ($b = 250$)

(c) MNIST$_{0\text{-}2}$ ($b = 2000$)

(d) MNIST$_{\text{hard}}$ ($b = 0$)

(e) MNIST$_{\text{hard}}$ ($b = 250$)

(f) MNIST$_{\text{hard}}$ ($b = 2000$)

Figure 6: (Color online) Underlying latent representations (l_{dae}) vs anomaly score (s_{dae}) for DAE_{uai} network as training progresses on MNIST$_{0\text{-}2}$ and MNIST$_{\text{hard}}$.

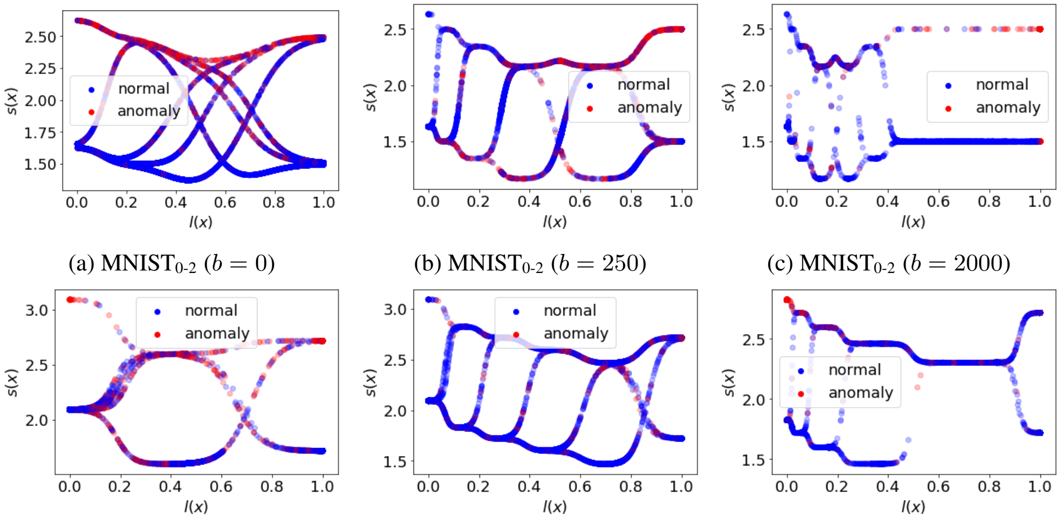

(a) MNIST$_{0\text{-}2}$ ($b = 0$)

(b) MNIST$_{0\text{-}2}$ ($b = 250$)

(c) MNIST$_{0\text{-}2}$ ($b = 2000$)

(d) MNIST$_{\text{hard}}$ ($b = 0$)

(e) MNIST$_{\text{hard}}$ ($b = 250$)

(f) MNIST$_{\text{hard}}$ ($b = 2000$)

Figure 7: (Color online) Underlying latent representations (l_{class}) vs anomaly score (s_{class}) for $Class_{uai}$ network as training progresses on MNIST$_{0\text{-}2}$ and MNIST$_{\text{hard}}$.

D Proofs

D.1 Lemma 1. Mixture probability lemma

Lemma 1. *Consider two independent arbitrary probability distributions p_1 and p_2. Given only a third distribution $p_+ = \overline{p}$ composed of the weighted average of the two:*

$$p_+ = (1 - \lambda) \cdot p_1 + \lambda \cdot p_2, \quad 0 \leq \lambda \leq 1$$

and considering P_i as the residual probability distribution hyperplanes:

$$\begin{aligned} P_1 &= \left\{ p_r = \frac{\overline{p} - \lambda \cdot p}{1 - \lambda}, \forall p \in P \mid \lambda \in [0; 1], \lambda \cdot p \leq \overline{p} \right\} \\ &= \left\{ p_r, \forall p_r \in P \mid \lambda \in [0; 1], (1 - \lambda) \cdot p_r \leq \overline{p} \right\} \end{aligned}$$

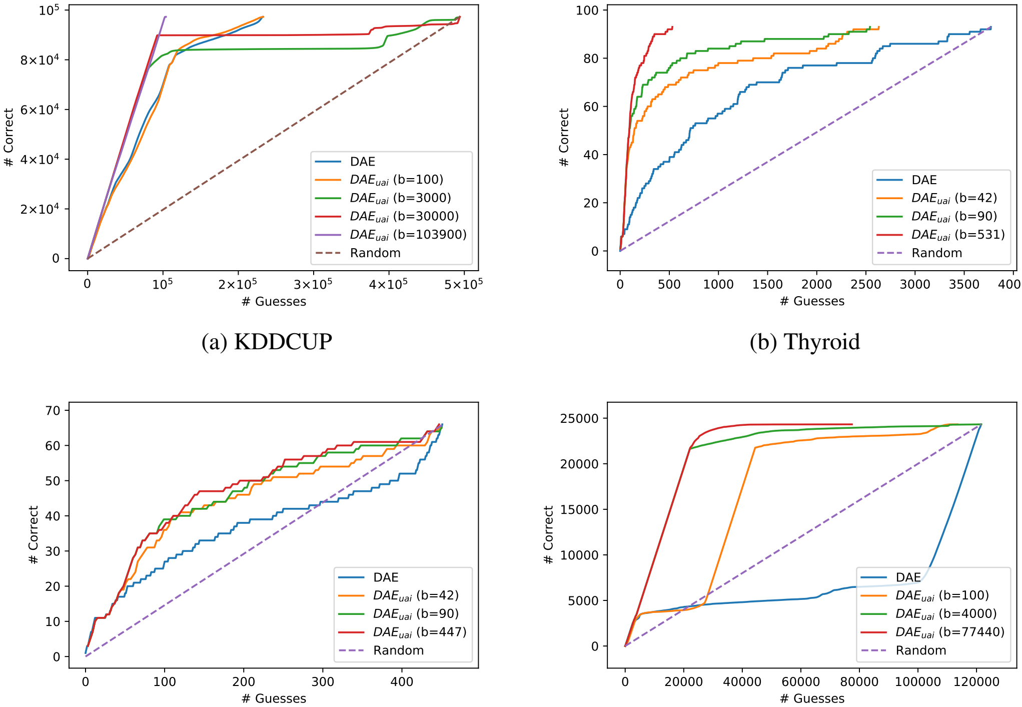

(a) KDDCUP

(b) Thyroid

(c) Arrhythmia

(d) KDDCUP-Rev

Figure 8: (Color online) Results for the real anomaly detection datasets when the UaiNets are only fed expert information until a budget (b) limit. Lines stop in the x-axis when all anomalies have been discovered.

$$\begin{aligned} P_2 &= \left\{ p_r = \tfrac{\overline{p}-(1-\lambda)\cdot p}{\lambda}, \forall p \in P \mid \lambda \in [0;1], (1-\lambda)\cdot p \leq \overline{p} \right\} \\ &= \{ p_r, \forall p_r \in P \mid \lambda \in [0;1], \lambda \cdot p_r \leq \overline{p} \} \end{aligned}$$

Without further assumptions on p_2 (without a prior on its probability distribution), we only know that $p(p_1|p_+ = \overline{p}) = p(p_1|p_1 \in P_1)$ and $p(p_2|p_+ = \overline{p}_\alpha) = p(p_1 = \overline{p}_\alpha - \lambda_\alpha \cdot p_2|p_2 \in P_2)$.

Proof. Given $p_+ = \overline{p}$ we know that:

$$p_1 + \lambda_\alpha \cdot p_2 = \overline{p}_\alpha$$

with $\lambda_\alpha = \frac{\lambda}{1-\lambda}$ and $\overline{p}_\alpha = \frac{\overline{p}}{1-\lambda}$. Assuming the distribution of p_2 is independent of p_1, and with no further assumptions on it, p_2 is random and uniform on the set of all possible probability distributions, so its probability distribution is:

$$p_2 \sim Uniform(P)$$

where P is the hyperspace containing all probability distributions, with an hyper-volume m. Now we can try to find $p(p_1|p_+ = \overline{p})$:

$$\begin{aligned}
p(p_1|p_+ = \overline{p}) &= p\left(p_+ = \overline{p}|p_1\right) \cdot \frac{p(p_1)}{p(p_+ = \overline{p})} \\
&\overset{(1)}{=} p\left(p_+ = \overline{p}|p_1\right) \cdot \frac{p(p_1)}{p(p_+ = \overline{p})} && , p_1 \in P_1 \\
&\overset{(2)}{=} p\left(p_2 = \frac{\overline{p}_\alpha - p_1}{\lambda_\alpha}|p_1\right) \cdot \frac{p(p_1)}{\displaystyle\int_x p\left(p_1 = x, p_2 = \frac{\overline{p}_\alpha - x}{\lambda_\alpha}\right) dx} \\
&\overset{(3)}{=} p\left(p_2 = \frac{\overline{p}_\alpha - p_1}{\lambda_\alpha}\right) \cdot \frac{p(p_1)}{\displaystyle\int_x p\left(p_1 = x, p_2 = \frac{\overline{p}_\alpha - x}{\lambda_\alpha}\right) dx} \\
&\overset{(4)}{=} \frac{1}{m} \cdot \frac{p(p_1)}{\displaystyle\int_x p\left(p_1 = x|p_2 = \frac{\overline{p}_\alpha - x}{\lambda_\alpha}\right) \cdot p\left(p_2 = \frac{\overline{p}_\alpha - x}{\lambda_\alpha}\right) dx} \\
&\overset{(5)}{=} \frac{1}{m} \cdot \frac{p(p_1)}{\displaystyle\int_{x \in P_1} p(p_1 = x) \cdot \frac{1}{m} dx + \int_{x \notin P_1} 0dx} \\
&= \frac{p(p_1)}{\displaystyle\int_{x \in P_1} p(p_1 = x)dx} \\
p(p_1|p_+ = \overline{p}_\alpha) &= p(p_1|p_1 \in P_1)
\end{aligned}$$

The equality in (1) comes from the definition of the space P_1, which is the space of all possible values of p_1 that could result in $p_+ = \overline{p}$, so if $p_1 \notin P_1$, then $p\left(p_+ = \overline{p}|p_1\right) = 0$. Equality (2) is a simple variable substitution where $p\left(p_+ = \overline{p}\right) = p\left(p_1 = x, p_2 = \frac{\overline{p}_\alpha - x}{\lambda_\alpha}\right)$. (3) comes from the assumption that p_2 and p_1 are independent. Equality (4) results from $p_2 \sim Uniform(P)$ and P having a volume m. Finally, Equality (5) is a result from the fact that $\dfrac{\overline{p}_\alpha - x}{\lambda_\alpha} \in P \Leftrightarrow x \in P_1$.

With a similar strategy we can find $p(p_2|p_+ = \overline{p})$:

$$\begin{aligned}
p(p_2|p_+ = \overline{p}) &= p(p_+ = \overline{p}|p_2) \cdot \frac{p(p_2)}{p(p_+ = \overline{p})} \\
&= p(p_1 = \overline{p}_\alpha - \lambda_\alpha \cdot p_2|p_2) \cdot \frac{p(p_2)}{\displaystyle\int_x p\left(p_1 = x, p_2 = \frac{\overline{p}_\alpha - x}{\lambda_\alpha}\right) dx} \\
&= p(p_1 = \overline{p}_\alpha - \lambda_\alpha \cdot p_2|p_2) \cdot \frac{p(p_2)}{\displaystyle\int_x p\left(p_1 = x, p_2 = \frac{\overline{p}_\alpha - x}{\lambda_\alpha}\right) dx} && , p_2 \in P_2 \\
&\overset{(1)}{=} p(p_1 = \overline{p}_\alpha - \lambda_\alpha \cdot p_2|p_2) \cdot \frac{p(p_2)}{\displaystyle\int_x p\left(p_1 = x, p_2 = \frac{\overline{p}_\alpha - x}{\lambda_\alpha}\right) dx} && , p_1 \in P_1 \\
&= p(p_1 = \overline{p}_\alpha - \lambda_\alpha \cdot p_2) \cdot \frac{p(p_2)}{\displaystyle\int_x p\left(p_1 = x, p_2 = \frac{\overline{p}_\alpha - x}{\lambda_\alpha}\right) dx} \\
&= p(p_1 = \overline{p}_\alpha - \lambda_\alpha \cdot p_2) \cdot \frac{\frac{1}{m}}{\displaystyle\int_x p\left(p_1 = x|p_2 = \frac{\overline{p}_\alpha - x}{\lambda_\alpha}\right) \cdot p\left(p_2 = \frac{\overline{p}_\alpha - x}{\lambda_\alpha}\right) dx} \\
&= p(p_1 = \overline{p}_\alpha - \lambda_\alpha \cdot p_2) \cdot \frac{\frac{1}{m}}{\displaystyle\int_{x \in P_1} p(p_1 = x) \cdot \frac{1}{m} dx + \int_{x \notin P_1} 0dx} \\
&= \frac{p(p_1 = \overline{p}_\alpha - \lambda_\alpha \cdot p_2)}{\displaystyle\int_{x \in P_1} p(p_1 = x)dx} \\
&= p(p_1 = \overline{p}_\alpha - \lambda_\alpha \cdot p_2|p_1 \in P_1) \\
&\overset{(2)}{=} p(p_1 = \overline{p}_\alpha - \lambda_\alpha \cdot p_2|p_2 \in P_2) \\
p(p_2|p_+ = \overline{p}) &= p(p_1 = \overline{p}_\alpha - \lambda_\alpha \cdot p_2|p_2 \in P_2)
\end{aligned}$$

where Equality (1) and (2) result from the fact that $p_1 \in P_1 \Leftrightarrow p_2 \in P_2$, given a specific value of $p_+ = \overline{p}$. This completes this proof. □

D.2 Lemma 2. Extreme mixtures lemma

Lemma 2. *Consider two independent arbitrary probability distributions p_1 and p_2. Given only a third probability distribution $p_+ = \overline{p}$ composed of the weighted mixture of the two, and for a small $\lambda \approx 0$, we can find a small residual hyperplane P_1, which tends to $\{\overline{p}\}$.*

$$P_1 \approx \{p_r = \overline{p} - \lambda \cdot p, \forall p \in P \mid \lambda \cdot p \leq \overline{p}\} \quad \lambda \approx 0 \tag{13}$$

We can also find a very large residual hyperplane P_2 for p_2, which tends to:

$$\lim_{\lambda \to 0} P_2 = \{p, \forall p \in P \mid supp(p) \subseteq supp(\overline{p})\} \tag{14}$$

where $supp(\cdot)$ is the support of a probability distribution.

Proof. In this proof, we start with the arbitrary residual hyperplanes P_r and find restrictions in the limits of $\lambda \to 0$ and $\lambda \to 1$. For a $\beta \approx 0$:

$$\begin{aligned}
\lim_{\beta \to 0} P_r &= \lim_{\beta \to 0}\{p_r = \tfrac{\overline{p} - \beta \cdot p}{1 - \beta}, \forall p \in P \mid \beta \cdot p \leq \overline{p}\} \\
&= \lim_{\beta \to 0}\{p_r = \overline{p} - \beta \cdot p, \forall p \in P \mid \beta \cdot p \leq \overline{p}\} \\
&= \{\overline{p}\} \\
P_r &\approx \{p_r = \overline{p} - \beta \cdot p, \forall p \in P \mid \beta \cdot p \leq \overline{p}\} && \beta \approx 0 \\
P_1 &\approx \{p_r = \overline{p} - \lambda \cdot p, \forall p \in P \mid \lambda \cdot p \leq \overline{p}\} && \lambda \approx 0 \\
P_2 &\approx \{p_r = \overline{p} - (1 - \lambda) \cdot p, \forall p \in P \mid (1 - \lambda) \cdot p \leq \overline{p}\} && \lambda \approx 1 \therefore \beta \approx 0
\end{aligned}$$

For a $\beta \approx 1$ we start with the other definition of P_r:

$$\begin{aligned}
\lim_{\beta \to 1} P_r &= \lim_{\beta \to 1}\{p_r, \forall p_r \in P \mid (1 - \beta) \cdot p_r \leq \overline{p}\} \\
&= \lim_{\beta \to 1}\{p_r, \forall p_r \in P \mid \text{supp}(p_r) \subseteq \text{supp}(\overline{p}), (1 - \beta) \cdot p_r \leq \overline{p}\} \\
&= \{p_r, \forall p_r \in P \mid \text{supp}(p_r) \subseteq \text{supp}(\overline{p})\} \\
P_r &\approx \{p_r, \forall p_r \in P \mid \text{supp}(p_r) \subseteq \text{supp}(\overline{p})\} && \beta \approx 1 \\
P_1 &\approx \{p_r, \forall p_r \in P \mid \text{supp}(p_r) \subseteq \text{supp}(\overline{p})\} && \lambda \approx 1 \\
P_2 &\approx \{p_r, \forall p_r \in P \mid \text{supp}(p_r) \subseteq \text{supp}(\overline{p})\} && \lambda \approx 0 \therefore \beta \approx 1
\end{aligned}$$

This finishes this proof. □

D.3 Theorem 3. No free anomaly theorem

Theorem 3. *Consider two independent arbitrary probability distributions p_{normal} and p_{anom}. For a small number of anomalies $\lambda \approx 0$, the knowledge that $p_{\mathit{full}} = \overline{p}$ gives us no further knowledge on the distribution of p_{anom}:*

$$p(p_{anom} | p_{\mathit{full}} = \overline{p}) \approx \mathit{Uniform}(P_2), \quad \lambda \approx 0$$

Proof. Consider in Theorems 1 and 2 that $p_2 = p_{anom} \sim \mathit{Uniform}(P)$. We then have that, for a small value of $\lambda \approx 0$:

$$\begin{aligned}
p(p_2 | p_+ = \overline{p}_\alpha) &= p(p_1 = \overline{p}_\alpha - \lambda_\alpha \cdot p_2 | p_2 \in P_2) \\
&\approx p(p_1 = \overline{p}_\alpha | p_2 \in P_2) \\
&= \mathit{Uniform}(P_2)
\end{aligned}$$

This finishes this proof. □

E Further Proofs

In this section, we prove upper and lower bounds on the maximum distance a probability distribution p_1 can be from p_+, based on the value of λ. This can be directly applied to p_{normal} for small values of λ and to p_{anom} for large ones.

Theorem 4. ***Upper Bound on Mixture Probability Distance*** *For two independent arbitrary probability distributions p_1 and p_2, given only a third probability distribution p_+ composed of the weighted mixture of the two:*

$$p_+ = (1-\lambda)\cdot p_1 + \lambda \cdot p_2$$

We have an upper bound on the distance measures $\delta(p_+, p_1)$ and $||p_+ - p_1||$ given by:

$$\delta(p_+, p_1) \leq \sqrt{\frac{1}{2}\log\frac{1}{1-\lambda}}$$

$$||p_+ - p_1|| \leq \sqrt{2\log\frac{1}{1-\lambda}}$$

which is a tight bound for $\lambda \approx 0$. In this equation $\delta(\cdot)$ is the total variation distance between two probability distributions and $||\cdot||$ is the L_1 norm.

Proof. Pinsker's inequality states that if p and q are two probability distributions on a common measurable space ($\mathcal{A}$, $\mathcal{F}$):

$$\delta(p,q) = \sup\{|p(A) - q(A)| \ : A \in \mathcal{F}\} \leq \sqrt{\frac{1}{2}\cdot D_{KL}\left(p||q\right)}$$

$$||p-q|| \leq \sqrt{2\cdot D_{KL}\left(p||q\right)}$$

where $D_{KL}\left(p||q\right)$ is the Kullback–Leibler divergence in nats. So we have that:

$$\delta(p_+, p_1) \leq \sqrt{\frac{1}{2}\cdot D_{KL}\left(p_1||p_+\right)}$$

and this Kullback–Leibler divergence is itself upper-bounded by:

$$\begin{aligned}
D_{KL}\left(p_1||p_+\right) &= \int_x \left(p_1(x)\log\tfrac{p_1(x)}{p_+(x)}dx\right) \\
&= \int_x \left(p_1(x)\log\tfrac{p_1(x)}{(1-\lambda)\cdot p_1(x)+\lambda\cdot p_2(x)}dx\right) \\
&\leq \max\nolimits_{p_2}\left(\int_x \left(p_1(x)\log\tfrac{p_1(x)}{(1-\lambda)\cdot p_1(x)+\lambda\cdot p_2(x)}dx\right)\right)
\end{aligned}$$

where this maximum Kullback–Leibler divergence is achieved when p_1 and p_2 are disjoint probability distributions:

$$\begin{aligned}
D_{KL}\left(p_1||p_+\right) &\leq \max\nolimits_{p_2}\left(\int_x \left(p_1(x)\log\tfrac{p_1(x)}{(1-\lambda)\cdot p_1(x)+\lambda\cdot p_2(x)}dx\right)\right) \\
&\leq \int_x \left(p_1(x)\log\tfrac{p_1(x)}{(1-\lambda)\cdot p_1(x)}dx\right) \\
&= \int_x \left(p_1(x)\log\tfrac{1}{1-\lambda}dx\right) \\
&= \log\tfrac{1}{1-\lambda}\int_x \left(p_1(x)dx\right) \\
&= \log\tfrac{1}{1-\lambda}
\end{aligned}$$

which concludes the proof that:

$$\delta(p_+, p_1) \leq \sqrt{\frac{1}{2}\log\frac{1}{1-\lambda}}$$

$$||p_+ - p_1|| \leq \sqrt{2\log\frac{1}{1-\lambda}}$$

□

Theorem 5. ***Lower Bound on Maximum Mixture Probability Distance*** *For two independent arbitrary probability distributions p_1 and p_2, given only a third probability distribution p_+ composed of the weighted mixture of the two:*

$$p_+ = (1-\lambda)\cdot p_1 + \lambda \cdot p_2$$

We have a lower bound on the maximum possible distance measures $\delta(p_+, p_1)$ and $||p_+ - p_1||$ for a chosen maximizing p_1 given by:

$$max_{p_1}\delta(p_+, p_1) \geq \lambda \cdot \frac{|\mathcal{A} - 1|}{|\mathcal{A}|}$$

$$max_{p_1}||p_+ - p_1|| \geq 2\lambda\frac{|\mathcal{A} - 1|}{|\mathcal{A}|}$$

which is a tight bound for $\lambda \approx 1$, considering the maximum L_1 distance between two probability distributions is 2.

Proof. We can prove a lower bound on the maximized distance of a probability distribution p_1 from p_+ by expanding the distance equations:

$$\begin{array}{rcl}
max_{p_1}\delta(p_+, p_1) & = & max_{p_1} \sup\{|p_+(A) - p_1(A)| \; : A \in \mathcal{F}\} \\
& = & max_{p_1} \sup\{|(1-\lambda) \cdot p_1 + \lambda \cdot p_2 - p_1(A)| \; : A \in \mathcal{F}\} \\
& = & max_{p_1} \sup\{|\lambda \cdot p_2(A) - \lambda \cdot p_1(A)| \; : A \in \mathcal{F}\} \\
& = & \lambda \cdot max_{p_1} \sup\{|p_2(A) - p_1(A)| \; : A \in \mathcal{F}\} \\
& \overset{\text{(a)}}{\geq} & \lambda \cdot max_{p_1} min_{p_2} \sup\{|p_2(A) - p_1(A)| \; : A \in \mathcal{F}\} \\
& \overset{\text{(b)}}{=} & \lambda \cdot max_{p_1} \sup\{|Uniform(\mathcal{A}) - p_1(A)| \; : A \in \mathcal{F}\} \\
& \overset{\text{(c)}}{=} & \lambda \cdot \sup\{|Uniform(\mathcal{A}) - \delta(A)| \; : A \in \mathcal{F}\} \\
& = & \lambda \cdot \frac{|\mathcal{A}-1|}{|\mathcal{A}|} \\
max_{p_1}\delta(p_+, p_1) & \geq & \lambda \cdot \frac{|\mathcal{A}-1|}{|\mathcal{A}|}
\end{array}$$

where in (a) we lower bound based on the probability distribution that would have the smallest possible superior distance to a later maximized probability distribution p_1. This probability distribution p_1 can always maximize its superior distance to p_2 by:

$$p_1(a) = \begin{cases} 1 & , if \; a = \text{argmin}_x(p_2(x)) \\ 0 & , else \end{cases}$$

In (b) we choose the uniform distribution as the one that would reduce this superior distance and in (c) we set $p_1(a) = 1$ for a random a, since p_2 is uniform. With a similar strategy we find:

$$max_{p_1}||p_+ - p_1|| \geq 2\lambda\frac{|\mathcal{A} - 1|}{|\mathcal{A}|}$$

This concludes this proof. □